https://doi.org/10.5194/tc-2022-27
Preprint. Discussion started: 23 March 2022

The Cryosphere Discussions

Environmental Conditions for Snow Cornice Formation tested in a Wind Tunnel

Hongxiang Yu[1,3,4], Guang Li[1,2,3,4], Benjamin Walter[4], Michael Lehning[3,4], Jie Zhang[1], and Ning Huang[1]

[1]College of Civil engineering and Mechanics, Lanzhou University, Lanzhou, 730000, China
[2]College of Atmospheric Science, Lanzhou University, Lanzhou, 730000, China
[3]College of Architecture Civil and Environmental Engineering, Ecole Polytechnique Federal de Lausanne, Lausanne, 1015, Switzerland
[4]WSL Institute for Snow and Avalanche Research SLF, Davos, 7260, Switzerland

Correspondence: Ning Huang (huangn@lzu.edu.cn)

Abstract. Snow cornices growing on the lee of mountain ridges are a common feature in alpine and polar regions during snow seasons. They can result in potential avalanche risk when they crack and fall. Current studies of cornices mainly focus on their deformation, collapsing, and avalanche risk via field observations. Few studies have paid attention to the accretion process of cornices, especially on their horizontal growth which enhances the instability of cornices. In this work, experiments in a cold laboratory under various wind conditions are carried out to investigate the environmental conditions and the internal physical mechanism of cornice formation. The results show that—for the specific settings in our wind tunnel—cornices appear only under moderate wind speeds which lead to necessary net mass flux divergence near the edge. The fastest growth rate is with winds approximately 40% higher than the rebound threshold wind speed for snow transport because then the snow mass supply to the cornice edge is sufficient. Mass collection efficiency on the cornice surface decreases with the increasing wind speed. This work improves our understanding of cornice formation.

1 Introduction

Snow cornices are leeward-growing masses of snow overhanging at the sharp breaks in slope, usually appearing on the ridgeline of steep mountains (Seligman et al., 1936). Some cornices deform, detach, and eventually fall off, which induces cornice fall avalanches or slope erosion, and leads to a redistribution of the snow cover below (Wahl et al., 2009). For example, cornice fall avalanches accounted for 45.2 % of all 423 snow avalanches observed in the Longyearbyen area, central Svalbard, from 2006 to 2009. They triggered slab avalanches (16.2 %) and loose snow avalanches (12.1 %) as secondary avalanches on the slope below (Eckerstorfer and Christiansen, 2011). These cornice fall avalanches cause potential threats to local infrastructures and human lives.

Cornice studies have attracted many contributions from Europe (Paulcke and Welzenbach, 1928; van Herwijnen and Fierz, 2014), America (Montagne, 1980; McCarty et al., 1986; Munroe, 2018), China (Zhizhong and Wenti, 1987), Japan (Kobayashi et al., 1988; Tsutsumi, 2005), and recently more in the Arctic (Vogel et al., 2012; Eckerstorfer et al., 2013; Hancock et al., 2020; Veilleux et al., 2021), due to the potential threats of cornice fall avalanches. Most of them are field observation studies

https://doi.org/10.5194/tc-2022-27
Preprint. Discussion started: 23 March 2022

using time-lapse photography or terrestrial laser scanner methods to record the development of cornices and analyse them through meteorological data. Most studies focused on the deformation and then collapse of cornices, as well as the ensuing cornice fall avalanches. Although understanding the initial evolution of cornices is a foundation of predicting and treating cornice fall avalanches, only a few studies have paid attention to the initial accretion process, especially to the horizontal extension forming the main part of snow mass overhanging the edge of a mountain crest. An indirect evidence was presented by van Herwijnen and Fierz (2014) that snow cornice only grows under moderate to high strength wind during or soon after the snowfalls, as well as the remarkable agreement between observed cornice width and the wind drift index calculated by the snow cover model SNOWPACK (Lehning and Fierz, 2008), which indicates that snow mass transport plays an important role in cornice formation. However, due to the coarse temporal resolution (normally hours or days) and uncontrollable weather conditions outside, dynamic details of snow mass transportation could not be recorded. Thus, the main reason for the horizontal growth of snow cornice remains unclear. In addition, several hypotheses were proposed to explain the cornice formation. Due to the wedged-like shape and typical appearance on cliffs where sudden changes of air pressure and wind velocity between accelerating windward slope and decelerating leeward slope are observed, the hypothesis was put forward that the reflux vortex structure of the lee-side flow field is the main reason of cornice formation (Seligman et al., 1936). Particles, which follow the changing wind direction locally as the flow passes the ridge will stick to the growing cornice front at the mountain ridge is a widely accepted hypothesis. Later, Latham and Montagne (1970) suggested that electrification may play an important role in cornice formation through observation of the electric field strength over a cornice. However, there is no evidence to support these assumptions so far. Thus, we present a wind tunnel experiment in a cold laboratory at WSL/SLF to investigate cornice formation processes. This work delivers the first insight into wind speed and mass concentration as factors influencing snow cornice accretion from a macroscopic view.

2 Methods

2.1 Experimental Setup

The experiments were carried out in a cold lab of the WSL Institute for Snow and Avalanche Research SLF (WSL/SLF) in Davos Dorf, Switzerland, where the room temperature could be controlled from −25 °C to 0 °C. An obround, closed-circuit wind tunnel built by Sommer et al. (2017, 2018) was used to perform the investigations. The room temperature of the cold lab was set to be a constant of −5 °C and the corresponding relative humidity inside the tunnel is in the range of 80–90 % during the following experiments.

The schematic diagram of the experimental setup is shown in Fig. 1. The wind tunnel contains two straight sections (length = 1 m, marked as S1 and S2) and two half-circle sections (outer diameter = 0.6 m, marked as H1 and H2). Its cross-section area is 0.2 m (width) × 0.5 m (height). An electric motor with rotor blades installed inside the middle of H1 creates the wind flow with a wind speed range of 0–7 m s^{-1}. A sieve is installed at S1 where the tunnel has an upward open window for the supply of snow particles. Sensors monitoring the air conditions are installed at the inlet of S2, and details are listed in Table1. The wind tunnel was cleaned before each test, and a ridge model made of compacted snow was built at S2. The shape and

https://doi.org/10.5194/tc-2022-27
Preprint. Discussion started: 23 March 2022

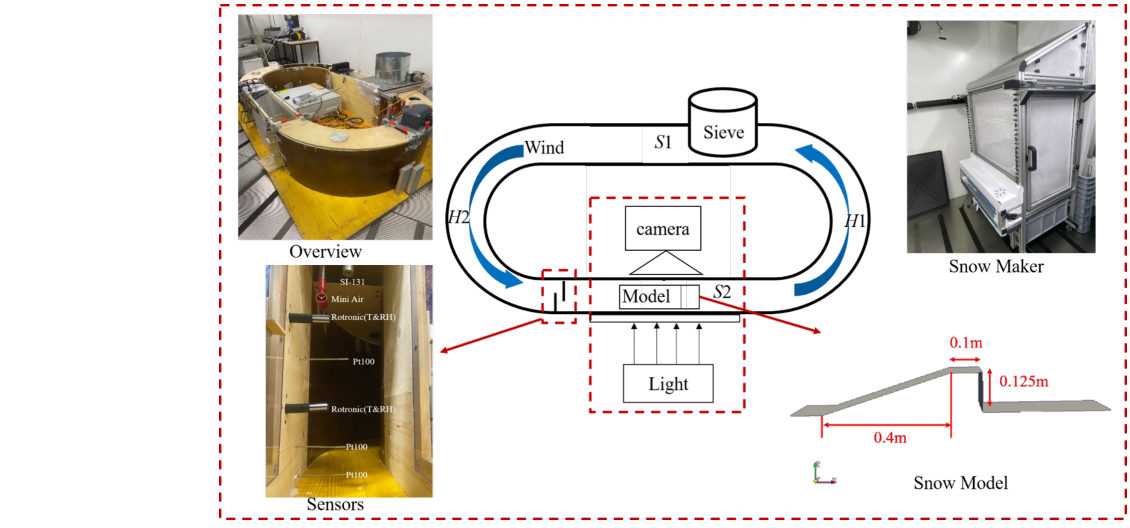

Figure 1. Schematic diagram of the closed-circuit tunnel experimental system in the cold lab. The insets are the pictures of the wind tunnel, Snow Maker , sensors, and the snow model set up inside the wind tunnel.

size of the ridge model affect the lee side eddy position and the snow particles' trajectories, which could have an influence on the experimental results. After multiple tests to present the best view of cornice growth, the size of the ridge model was set as 0.125 m in height and with a 0.1 m flat section (Fig. 1). The angle of the slope relative to the horizontal direction is 36°. To record the growth of the cornice using shadowgraphy imaging, we placed a CMOS Camera with a spatial resolution of 2048 × 2048 pixels to zoom on the edge of the ridge area and placed a LED lamp on the opposite side as a light source.

Fresh snow particles made by a snowmaker developed by SLF (Schleef et al., 2014) were used for feeding the flow through the sieve. When using the snowmaker, the room temperature was set to −20 °C, and the water inside the reservoir was set to +30 °C for the snowmaker. The obtained fresh snow is a mixture of dendritic crystals and hollow columns. Its density was measured by an electronic balance before each wind tunnel experiment, and the mean value was 149 kg m^{-3}. Its average diameter estimated by a grid plate and the amplifying lens was about 500 μm, and the specific surface area (SSA) measured by μCT is 75 mm^{-1} (Schleef et al., 2014). A constant seeding rate has been applied for all experiments.

Rebound threshold wind speed in the experiment is determined 1) by seeding fresh snow, increasing the wind speed from zero until saltation particles can be observed; 2) decrease the wind speed slowly, until there are no saltating snow particles visible anymore while still sieving fresh snow into the tunnel. The average wind speed at these two times is considered as the rebound threshold wind speed correspondingly (Walter et al., 2014). The average value of rebound threshold wind speed was found to be 3.2 m s^{-1} at the height of the mini-air. Thus, seven target wind speed conditions (from 3.0 m s^{-1} to 6.5 m s^{-1} by steps of 0.5 m s^{-1}) were set for the experiments. The target wind speed value is set in the control system before each experiment. The actual wind speed increases continually after the electric motor rotates the propeller until it reaches the target wind speed. The propeller speed is adjusted throughout the experiment to keep the wind speed constant in case larger snow particles depositions

https://doi.org/10.5194/tc-2022-27
Preprint. Discussion started: 23 March 2022


The Cryosphere Discussions
Open Access
EGU

Table 1. Instruments, variables, and data acquisition interval.

Instrument	Instrument model	Variables	Time interval
CMOS Camera	LP285-40.5	Images	0.02s
Wind Speed Tester	Mini Air	U (m s^{-1})	0.2s
Snow Temperature	Pt100	T_{S} (K)	1s
Snow Surface Temperature	SI-131	T (K)	1s
Air Temperature and RH	Rotronic	T (K) and RH (%)	1s

alter the flow situation inside the wind tunnel. After the experiments, the particle mass concentration, cornice length, cornice volume, and growth rate were obtained by image processing of the series of pictures.

2.2 Image Processing

The CMOS camera recorded 50 images with 10 Hz frequency in the burst mode, and the pause between two bursts was 5 s. Thus, 50 continuous frames in 5 s as one set were obtained, which could be used to estimate the cornice growth rate and transport mass flux instantaneously or on average. The field of view was 7.7 cm $\times$ 7.7 cm, and the depth of field was 3.5 cm for particles with the mean size of 500 μm, which are calibrated by using the method of Crivelli et al. (2016). The first image, in which only the model crest was visible without snow particles moving across, was set as a background image, as shown in Fig. 2(a). For a set of 50 frames, we first subtracted the background image and then transformed the result to binary format (where pixels with snow is 1, and without snow is 0), as shown in Fig. 2(c) and (d). During this process, a high threshold value V1 was predefined for only presenting cornice shape without snow particles in the air. Then, the continuous value of 1 in each row/column was counted, and its maximum values defined the cornice thickness/length. The instantaneous cornice growth rate is then calculated by the difference of two adjacent frames divided by 0.1 s, and the averaged cornice growth rate is the mean value of the instantaneous cornice growth rates in one set of 5 s. The thickness of accumulated snow represents the net amount of deposition and erosion, and the length growth rate of cornice represents the horizontal extension speed from the edge.

A window Ω with an area of 1 cm $\times$ 1 cm slightly above the snow cornice is chosen to calculate the mass fluxes to avoid errors due to surface effects and background light problems, shown in Fig. 2(b). The mass concentration of snow particles is calculated by predefining a low threshold value V2 which could clearly present the airborne snow particles, shown as Fig. 2(e). Ignoring the overlapping particles, we calculate the volume of snow particles in Ω as the orthographic projection area of snow particles multiplied by its average diameter. Thus, the mass concentration ϕ_{P} can be estimated as:

$$\phi_{\mathrm{P}} = \frac{\rho_{\mathrm{i}} \overline{d_{\mathrm{P}}} \Sigma_{\Omega} g_j A_0}{S_0 \times p} \tag{1}$$

https://doi.org/10.5194/tc-2022-27
Preprint. Discussion started: 23 March 2022

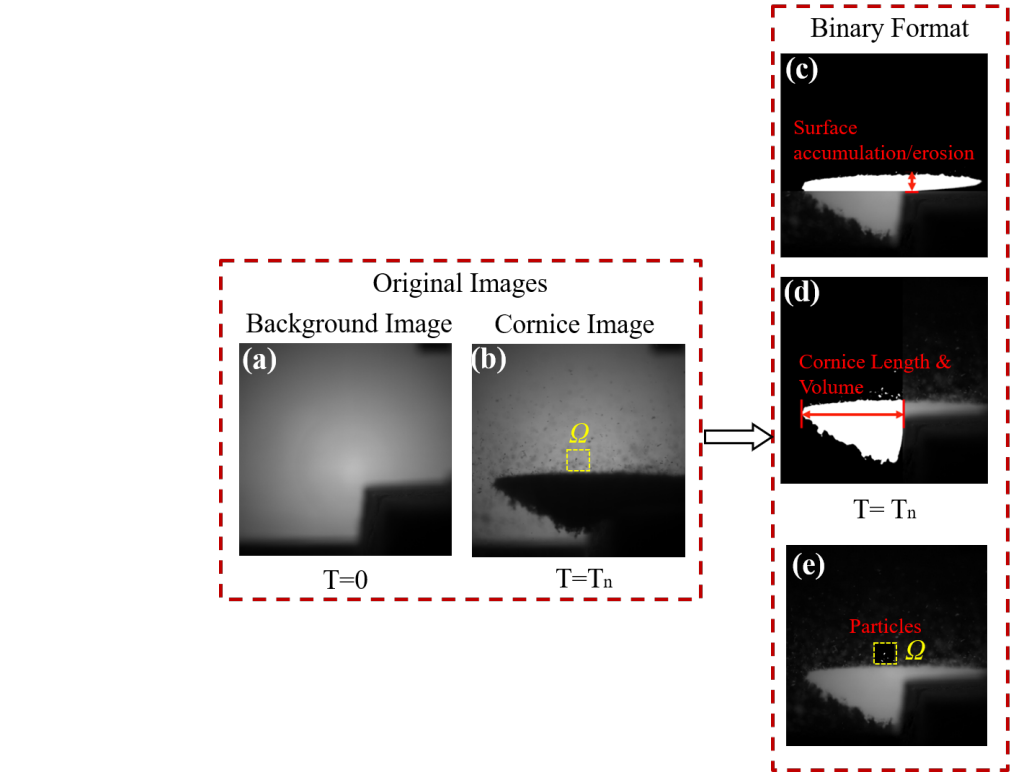

Figure 2. Post-Processing images using the grayscale method. (a)-(b) Raw images of background and cornice. (c)-(d) Binary format of images with information of the amount of accumulation/erosion and cornice length and volume. (e) Airborne snow particles captured in window Ω.

where ρ_i is the ice density, $\overline{d_P}$ is the averaged diameter, g_j is the binary value of the j^{th} pixel in window Ω, $A_0 = \frac{7.7\times7.7}{2048\times2048}$ cm^2 is the area of a pixel, $S_0 = 1$ cm^2 is the area of the window Ω, $p = 3.5$ cm is the depth of field where particles can be recognized in this width range.

3 Results and discussions

3.1 General observations on snow cornice formation

Using the case of $U = 4$ m s^{-1} as an example, Figure 3(a) shows the cornice size information associated with wind velocity and particle mass concentration. The wind speed (black squares) increased from 0 to 4 m s^{-1} in about 210 s and was then kept stable during the cornice formation process. The particle mass concentration (blue circles) started to increase at $t = 176$ s and reaches a stable value at $t = 250$ s. A cornice started to form approximately at the same time as the drifting snow occurred with a detectable particle mass concentration. Its length (red triangles) and volume (green triangles) almost linearly increased during the stage with a stable snow concentration ($\sim$ 1.4 kg m^{-3}) and wind speed ($\sim$ 4 m s^{-1}). During the cornice accretion

https://doi.org/10.5194/tc-2022-27
Preprint. Discussion started: 23 March 2022

The Cryosphere Discussions

time, the cornice grew both in length and thickness, and the profiles of the cornice in different time stages are shown in the inset of Fig. 3(a). Its maximum length growth rate is 3.2×10^{-4} m s^{-1}, and the average length growth rate during the stable wind speed is 1.4×10^{-4} m s^{-1}. For comparison, in field observations, the measured accretion rate range is 3.9×10^{-6} – 4.7×10^{-6} m s^{-1}(Hancock et al., 2020) which is two orders of magnitude smaller than the experimental values. The main reason for the discrepancies between the laboratory and the field results is most likely due to observational differences. The wind speed for cornice formation in the wind tunnel is continuous and stationary, while it is fluctuating and intermittent in the field, which causes the effective time for cornice formation being much less in the field than the sampling time (several hours to days).

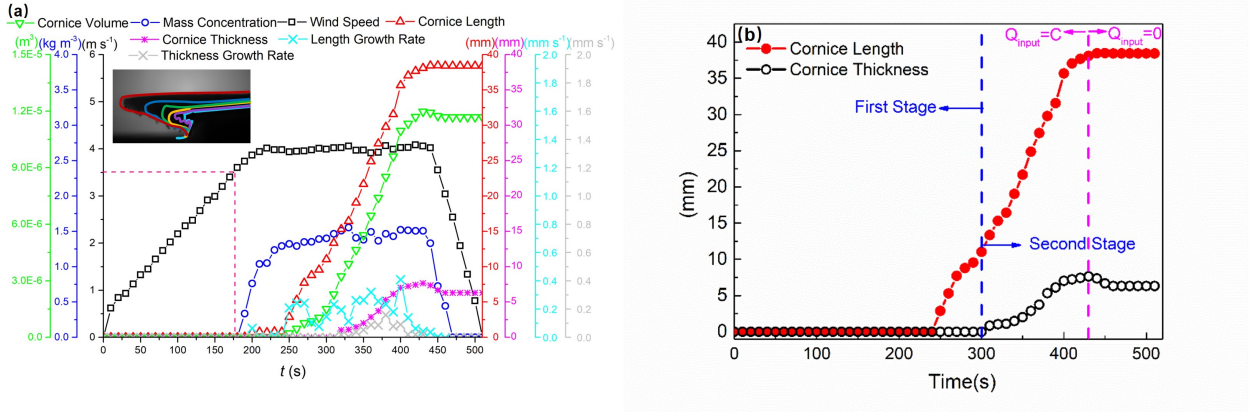

Figure 3. Variation of cornice length (red triangles), cornice thickness (pink squares), cornice volume (green triangles), cornice length growth rate (light blue triangles), cornice thickness growth rate (grey triangles), wind speed (black squares) and particle mass concentration in the air (blue circles). Inset includes cornice profiles during different growth periods. (b)Two stages of cornice length (red circles) and thickness (black circles) growth for U = 4 m s^{-1}. (T_{air} = –5 °C, U = 4 m s^{-1})

During cornice accretion, there are two stages for the growth of cornice. As shown in Fig. 3(b), the red circles represent the length of the cornice, and the black circles represent the thickness of accumulated snow above the cornice. In the first stage, a 0.011 m small slab forms outward from the edge of the ridge model with a horizontal growth rate that is much higher than the vertical growth rate. In the second stage, the cornice length and thickness simultaneously increase together and gradually reach a final length and final height until seeding ends. Once the seeding stops (t = 430 s), mass flux disappears when stopping seeding because the redistribution of the snow depositions in the wind tunnel results in a surface morphology inhibiting aerodynamic entrainment. The aerodynamic entrainment happens on the newly formed cornice surface because the surface shear stress is over the threshold value. In this case, the aerodynamic entrainment only scours the thickness of the cornice.

3.2 Suitable Wind Speed Range for Cornice Formation

Cornice formation was tested with wind speeds from 3 m s^{-1} to 6.5 m s^{-1} using 0.5 m s^{-1} increments. Mean cornice growth rates under all wind conditions were obtained by estimation of the slopes of the near-linear growth curves. As mentioned in Section

https://doi.org/10.5194/tc-2022-27
Preprint. Discussion started: 23 March 2022

The Cryosphere Discussions

3.1, erosion on the newly formed snow cornice happens after stopping seeding for $U > 3.5$ m s^{-1}. Therefore, in this section, we separately analysed the cornice growth rates (in length and in thickness) with seeding and the erosion rates (in length and in thickness) after seeding ended for each wind speed through a series of images shown as Fig. 4(a).

The growth rates in length and thickness can both be approximated by a quadratic function and reach the maximum value at moderate wind speeds (4–4.5 m s^{-1}). The erosion rates in length and thickness exponentially increase with the wind speed. In the cornice growing process, the length growth rate is faster than the thickness growth rate in each kind of wind. Once the wind speed is above 4 m s^{-1}, the erosion in length doesn't happen until the cornice has been eroded in thickness down to the original ridge model. This phenomenon indicates that the thickness erosion rate is always faster than the length erosion rate, which means that cornice surface thickness growth rate is more sensitive to erosion than the length growth rate.

There is no cornice formation for wind speeds equal to 3 m s^{-1} because of a missing saltation layer and snow transport. For wind speeds higher than 6 m s^{-1}, there are even no more chances for slabs to form on edge anymore because of continuous erosion on the model surface. Moreover, it can be concluded that the thickness growth rate decreases with increasing wind velocity as net deposition on the surface get smaller. The cornice length grows fastest when the wind speed value is approximately 40% higher than the rebound threshold wind speed in our case(Fig. 4(a)). The results show that drifting snow at moderate wind

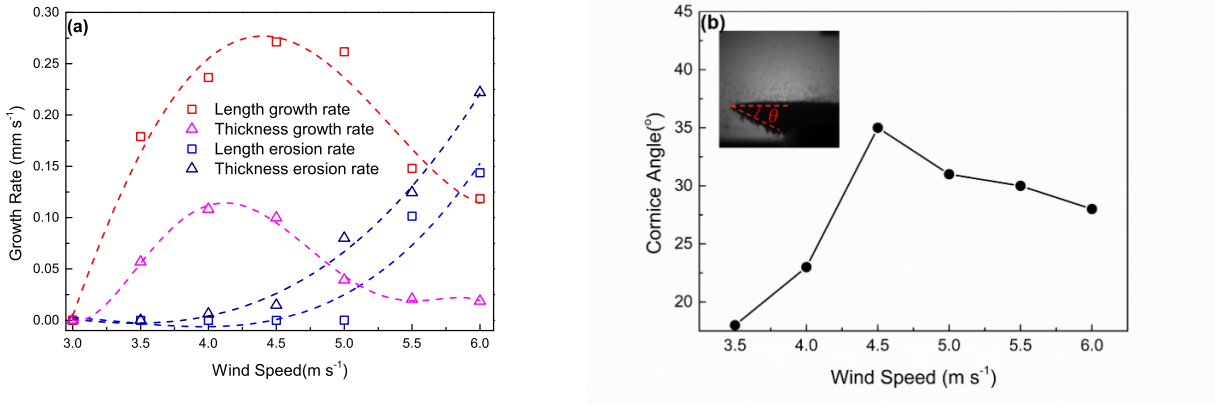

Figure 4. (a) Growth rate (in red) and erosion rate (in blue) in length (in squares) and in thickness (in triangles) under different wind speed conditions. (b) Angle θ of snow cornice in wind speeds of 3.5 m s^{-1}–6 m s^{-1}.

speed is needed for cornice formation, where a similar conclusion can be found from field observations (Vogel et al., 2012; Eckerstorfer et al., 2013; McClung and Schaerer, 2006; Montagne, 1980). Overall, the wind speed ranges discussed above depend on the properties of drifting snow and the friction velocity affected by the local topography.

Moreover, the interplay between deposition and erosion determines the final shape of cornices. In our experiment, the cornices are wedged-like with an angle of 18° to 35° shown in Fig. 4(b), which is consistent with field observations. The angle of the cornice is one of the factors that determine cornice stability. Smaller angles increase the danger of crackdown. In our

https://doi.org/10.5194/tc-2022-27
Preprint. Discussion started: 23 March 2022

145 experiment, the most stable structure is formed by moderate wind. The higher the wind speed is, the more unstable the cornice becomes.

Since the magnitude of drifting snow is critical for the vertical and horizontal cornice growth rates, snow mass transport rates were calculated for the different experiments and analysed in terms of mass exchange between the cornice and the saltation layer. The results were compared to field data to underline the relevance of our results for actual outdoor conditions. First, the
150 transport mass flux q_P can be estimated using:

$$q_P(z) = \phi_P(z)\overline{u}_P(z = 0.4) \tag{2}$$

where $\phi_P(z)$ is the mass concentration calculated by Eq. (2), and $\overline{u}_P$ is the averaged particle velocity, which is assumed to be 10% lower than wind speed (Nishimura et al., 2014). Thus, mass flux variation with height over snow cornices can be estimated by multiple windows Ω that are continuously distributed in height under different wind conditions, as is shown in Fig. 5. For
155 all wind conditions, the mass flux exponentially decreases with increasing height, which is consistent with previous results (Takeuchi, 1980; Lehning et al., 2002; Kosugi et al., 2008; Lü et al., 2012; Crivelli et al., 2016; Melo et al., 2022). It also increases overall with the increasing wind speed.

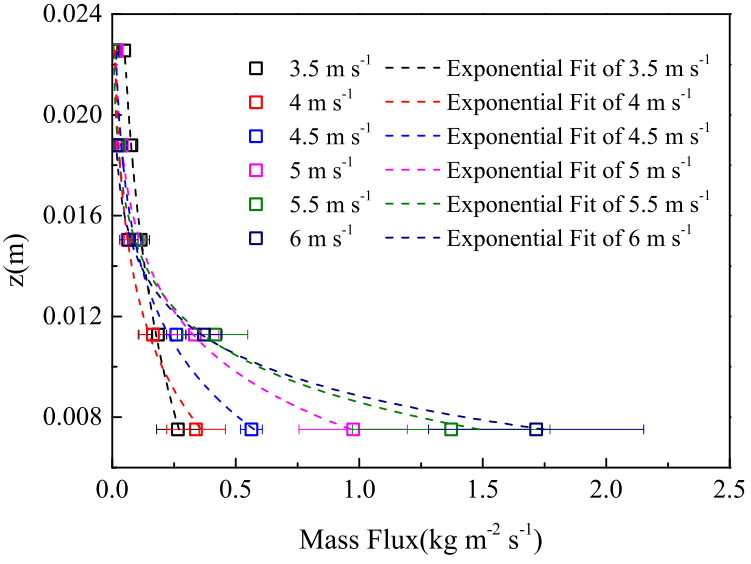

Figure 5. Mass flux variation with height under different wind conditions (3.5 m s^{-1}–6 m s^{-1}).

The transport mass flux profile can be described by an exponential law (Nishimura and Nemoto, 2005; Sugiura et al., 1998):

160 $$q_P(z) = Ae^{-R_0 z} \tag{3}$$

https://doi.org/10.5194/tc-2022-27
Preprint. Discussion started: 23 March 2022

The Cryosphere Discussions
Open Access
EGU

Table 2. Coefficients of A and R_0 in different wind speeds U.

Wind Speed U (m s^{-1})	A	R_0
3.5	0.62	109.42
4	2.09	218.5
4.5	3.63	245.32
5	8.44	288.16
5.5	24.05	370.31
6	40.72	418.78

where A and R_0 are constants that change with wind speed. By fitting Eq. (3) using the estimated transport mass flux from the shadow images, we obtain A and R_0 for different wind speeds, as summarized in Table 2. Their fitted functions are: A = −2092 + 1840U −596U^2 + 84U^3 −4U^4 and R_0 = −285.95 + 118.29U.

The transport rate can be expressed as:

$$Q = \int_0^\infty q_{\mathrm{P}}(\mathrm{z})dz = \int_0^\infty Ae^{-R_0 z}dz = -\frac{A}{R_0}e^{-R_0 z}|_{z=0}^{z=\infty} = \frac{A}{R_0} = \frac{-2092 + 1840U - 596U^2 + 84U^3 - 4U^4}{-285.95 + 118.29U} \quad (4)$$

by integrating the mass-flux profiles over height. To quantify the exchange of snow between the mass flux and the cornice, we defined the mass flux collection efficiency as:

$$E = \frac{S_{\mathrm{cornice}} \times \rho_{\mathrm{ice}}}{Q_{\mathrm{drift}}} \times 100\% \quad (5)$$

where $S_{\mathrm{cornice}} = \frac{dA_{\mathrm{c}}}{dt}$ is the growth rate of the cornice projected area A_{c}, therefore including horizontal and vertical growth. As is shown in Fig. 6, the maximum collection efficiency appears for the minimum wind speed of 3.5 m s^{-1}. With increasing wind speed and drift rate, the collection efficiency of snow particles on the cornice decreases.

According to Hancock et al. (2020), the appropriate wind speed range of cornice growth in the field is 12–30 m s^{-1} (in a height of 2.8 m). To compare it with our experiments, the mass concentration in this wind speed range was estimated by the following steps for our experiments:

1) Dimensionless snow transport rate on the flat surface $\tilde{Q} = \frac{gQ}{\rho_{\mathrm{a}} u_{*\mathrm{t}}^3}$ can be calculated as a function of the dimensionless wind velocity $\tilde{u} = \frac{u_*}{u_{*\mathrm{t}}} = \frac{U}{U_{\mathrm{t}}}$, where $u_{*\mathrm{t}}$ = 0.25 m s^{-1} is the threshold friction velocity Leonard et al. (2012), U_{t} is the corresponding threshold wind speed at a certain height ($U_{\mathrm{t0.4}}$ = 3.2 m s^{-1} in wind tunnel and $U_{\mathrm{t2.8}}$ = 11 m s^{-1} in field), ρ_{a} = 1.23 kg m^{-3} is the air density. Several common formulas of the function are shown in Table 3.

2) Blowing snow particle concentration in the air can be calculated as Pomeroy and Gray (1990):

$$\phi_{\mathrm{sal}} = \frac{Q}{h_{\mathrm{sal}} U_{\mathrm{sal}}} \quad (6)$$

https://doi.org/10.5194/tc-2022-27
Preprint. Discussion started: 23 March 2022

The Cryosphere Discussions
Open Access
EGU

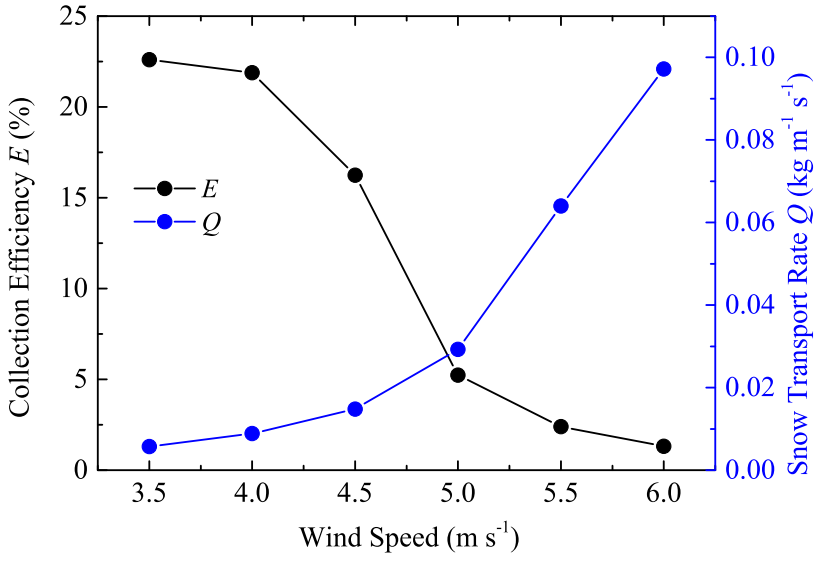

Figure 6. Collection efficiency E (black circles) and snow transport rate Q (blue circles) under different wind speeds.

Table 3. Dimensionless snow transport rate, $\tilde{Q}$

Dimensionless Transport Rate	Author and Year
$\tilde{Q} = C\sqrt{\frac{\langle d \rangle}{d_R}}\tilde{u}^3, C = 2.8(\text{non-uniform size}), C = 1.5(\text{uniform size})$	Bagnold, 1941
$\tilde{Q} = \tilde{u}^3(1 - \frac{1}{\tilde{u}^2})(2.6 + 2\frac{1}{\tilde{u}} + 2.5\frac{1}{\tilde{u}^2})$	Sørensen, 2004
$\tilde{Q} = \tilde{u}^3(1 - \frac{1}{\tilde{u}^2})(3.7 + 4.7\frac{1}{\tilde{u}} - 4\frac{1}{\tilde{u}^2})$	Li et al., 2018
$\tilde{Q} = C(\tilde{u}^2 - 1), C = 8.5$	Durán et al., 2011

d_R = 250 μm is the reference diameter, $\langle d \rangle$ is the average value of diameter.

where saltation height and saltation layer wind speed can be expressed as:

$$h_{sal} = 1.6\frac{u_*^2}{2g} \tag{7a}$$

$$U_{sal} = 2.8u_{*t} \tag{7b}$$

After substituting Eq. (7a) and Eq. (7b) into Eq. (6), the saltation particle mass concentration can be expressed as:

$$\tilde{\phi}_{sal} = \frac{\phi_{sal}}{\rho_a} = \frac{\tilde{Q}}{2.24\tilde{u}^2} \tag{8}$$

https://doi.org/10.5194/tc-2022-27
Preprint. Discussion started: 23 March 2022

The Cryosphere Discussions
Open Access
EGU

Figure. 7 shows the comparison of mass concentration between field situations and our wind tunnel conditions. When $1.1 < \tilde{u} < 1.9$, the mass concentration values in the wind tunnel are of the same order of magnitude as the estimated results of field situations (Bagnold, 2012; Sørensen, 2004; Li et al., 2018). However, due to the limit and size influence of the ring wind tunnel itself, the local wind speed on top of the cornice surface increases due to a reduction of the wind tunnel cross-section. Thus, when $\tilde{u} > 1.9$, the mass concentration in the wind tunnel experiment has already reached the value of that in site observation with $\tilde{u} \approx 2.6$, which results in the severely scouring and erosion on the model edge, which may not commonly happen in nature.

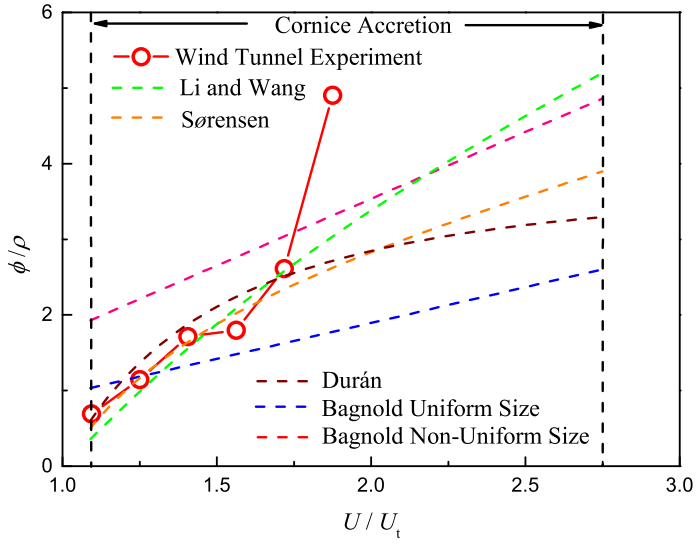

Figure 7. Dimensionless particle concentration in different wind velocity conditions. Dash lines in colours represent the field experiment values in different models, and the red circles represent the wind tunnel experiment values.

For the wind tunnel experiment and the natural situation, neither weak wind ($\tilde{u} < 1.1$) nor strong wind ($\tilde{u} > 2.7$) is suitable for the cornice growth, and only under moderate wind speed ($1.1 \leq \tilde{u} < 2.7$) cornices grow. This result is in good agreement with the other field observation results with the wind speed ranges of 10–32.4 m s^{-1} (Vogel et al., 2012; Eckerstorfer et al., 2013; McClung and Schaerer, 2006; Montagne, 1980). Thus, our wind tunnel experiment reflects the necessary mass concentrations of natural situations for cornice growth. The lower/upper limit of the friction velocity for cornice growth can be estimated, which can be helpful for the prediction of cornice formation and collapse. For example, in the case of $z_0 = 6.3 \times 10^{-5}$ m (Nishimura and Nemoto, 2005), the corresponding proper friction velocity range for the natural situation is 0.45–1.12 m s^{-1}, and when the friction velocity $u_* > 1.12$ m s^{-1} ($U > 30$ m s^{-1}), snow cornice surface starts being scoured by wind or cracked off which leads to a snow mass loss.

https://doi.org/10.5194/tc-2022-27
Preprint. Discussion started: 23 March 2022


The Cryosphere Discussions
Open Access
EGU

4 Conclusions and Outlook

This manuscript introduced the first wind tunnel experiment of the snow cornice accretion process, investigated by applying the method of shadow photography. In our experiments, snow cornices only grow at moderate wind speed (3.5–6 m s^{-1}) with sufficient snow mass flux over the ridge of the model. The final shape of the cornice is wedge-like due to the different growth rates in horizontal and vertical directions. The vertical growth was found to be typically lower relative to horizontal growth. Erosion of newly formed cornice starts for wind speeds higher than 4 m s^{-1} and first reduces the thickness of the cornice. The most favorable wind condition in the experiment for cornice growth is 4.5 m s^{-1}, which is approximately 40 % higher than the threshold wind speed for snow transport. Mass collection efficiency, reflecting particulate matter exchanges between the air and the ground surface, is put forward in this work. During the experiment, the mass collection efficiency decreases with the increasing wind speed and the corresponding drift rate. A comparison of the mass concentration during snow drifting in the wind tunnel and field experiments under the corresponding wind conditions shows that our experimental results, when properly non-dimensionalised, represent environmental conditions for cornice formation.

This work is a preliminary quantitative investigation of snow cornice formation. More detailed studies on the deposition process on snow cornices should be conducted in the future, e.g., As one of the main meteorological factors, the temperature will also potentially impact cornice formation. For example, higher environmental temperature could enhance fast sintering, which may be an essential mechanism. Still, it could also decrease air mass flux due to the stronger cohesion force, making it more difficult for particle entrainment. In this manuscript, we only take one kind of temperature T = -5°C as an example and will study the temperature influence in the future. Wind speeds for which value the growth rate reaches its maximum and the wind speed limit for cornice growth may differ for different temperatures and particle shapes. According to previous studies, the electrostatic force of snow particles may also play a significant role but hasn't been confirmed yet. The shape of the ridge model should be another critical factor due to the different turbulent structures produced behind the leeward area. To investigate these influencing factors, high-speed images of snow particle motion over snow cornices would be helpful.

Author contributions. YHX, LG, and BW designed the experiments. YHX and LG carried out the experiments, performed the data analysis, and prepared the first draft. ML, ZJ, and BW reviewed and edited the paper. HN and ML organized this study, contributed to its conceptualization, discussion, and finalized the paper.

Competing interests. The authors declare that they have no conflict of interest.

Acknowledgements. The authors would like to thank Dr. Matthias Jaggi for his Snow Maker expertise. The authors appreciate Dr. Mahdi Jafari and Daniela Brito Melo for the valuable suggestions to improve the manuscript. This work was supported by the National Natural Science Foundation of China (grant no.: 41931179 and 42006187), the Second Tibetan Plateau Scientific Expedition and Research Program

https://doi.org/10.5194/tc-2022-27
Preprint. Discussion started: 23 March 2022

(grant no.: 2019QZKK020109-2), the Fundamental Research Funds for the Central Universities (grant no.: lzujbky-2021-it29 and lzujbky-2020-pd11). And the data and code will be upload to Dryad repository after the paper is published.

https://doi.org/10.5194/tc-2022-27
Preprint. Discussion started: 23 March 2022

References

Bagnold, R. A.: The physics of blown sand and desert dunes, Courier Corporation, 2012.

Crivelli, P., Paterna, E., Horender, S., and Lehning, M.: Quantifying particle numbers and mass flux in drifting snow, Boundary-Layer Meteorology, 161, 519–542, https://doi.org/10.1007/s10546-016-0170-9, 2016.

Eckerstorfer, M. and Christiansen, H. H.: Topographical and meteorological control on snow avalanching in the Longyearbyen area, central Svalbard 2006–2009, Geomorphology, 134, 186–196, https://doi.org/10.1016/j.geomorph.2011.07.001, 2011.

Eckerstorfer, M., Christiansen, H., Rubensdotter, L., and Vogel, S.: The geomorphological effect of cornice fall avalanches in the Longyeardalen valley, Svalbard, The Cryosphere, 7, 1361–1374, https://doi.org/10.1002/esp.3292, 2013.

Hancock, H., Eckerstorfer, M., Prokop, A., and Hendrikx, J.: Quantifying seasonal cornice dynamics using a terrestrial laser scanner in Svalbard, Norway, Natural Hazards and Earth System Sciences, 20, 603–623, https://doi.org/10.5194/nhess-20-603-2020, 2020.

Kobayashi, D., Ishikawa, N., and Nishio, F.: Formation process and direction distribution of snow cornices, Cold Regions Science and Technology, 15, 131–136, https://doi.org/10.1016/0165-232X(88)90059-6, 1988.

Kosugi, K., Sato, T., Nemoto, M., Mochizuki, S., Sato, A., and Prevention, D.: Vertical profiles of mass flux for different particle diameters in drifting snow over hard snow surfaces, Proceeding of the ISSW, 38, 143–152, 2008.

Latham, J. and Montagne, J.: The possible importance of electrical forces in the development of snow cornices, Journal of Glaciology, 9, 375–384, https://doi.org/10.3189/S0022143000022899, 1970.

Lehning, M. and Fierz, C.: Assessment of snow transport in avalanche terrain, Cold Regions Science and Technology, 51, 240–252, https://doi.org/10.1016/j.coldregions.2007.05.012, 2008.

Lehning, M., Naaim, F., Naaim, M., Brabec, B., Doorschot, J., Durand, Y., Guyomarc'h, G., Michaux, J.-L., and Zimmerli, M.: Snow drift: acoustic sensors for avalanche warning and research, Natural Hazards and Earth System Sciences, 2, 121–128, https://doi.org/10.5194/nhess-2-121-2002, 2002.

Leonard, K. C., Tremblay, L.-B., Thom, J. E., and MacAyeal, D. R.: Drifting snow threshold measurements near McMurdo station, Antarctica: A sensor comparison study, Cold Regions Science and Technology, 70, 71–80, https://doi.org/10.1016/j.coldregions.2011.08.001, 2012.

Li, G., Wang, Z., and Huang, N.: A snow distribution model based on snowfall and snow drifting simulations in mountain area, Journal of Geophysical Research: Atmospheres, 123, 7193–7203, https://doi.org/10.1029/2018JD028434, 2018.

Lü, X., Huang, N., and Tong, D.: Wind tunnel experiments on natural snow drift, Science China Technological Sciences, 55, 927–938, https://doi.org/10.1007/s11431-011-4731-3, 2012.

McCarty, D., Brown, R., and Montagne, J.: Cornices: their growth, properties, and control, in: International Snow Science Workshop, Lake Tahoe, pp. 41–45, 1986.

McClung, D. and Schaerer, P. A.: The avalanche handbook, The Mountaineers Books, 2006.

Melo, D. B., Sharma, V., Comola, F., Sigmund, A., and Lehning, M.: Modeling snow saltation: the effect of grain size and interparticle cohesion, Journal of Geophysical Research: Atmospheres, 127, e2021JD035 260, 2022.

Montagne, J.: The University Course in Snow Dynamics—A Stepping-Stone to Career Interests in Avalanche Hazards, Journal of Glaciology, 26, 97–103, https://doi.org/10.3189/S0022143000010637, 1980.

Munroe, J. S.: Monitoring snowbank processes and cornice fall avalanches with time-lapse photography, Cold Regions Science and Technology, 154, 32–41, https://doi.org/10.1016/j.coldregions.2018.06.006, 2018.

https://doi.org/10.5194/tc-2022-27
Preprint. Discussion started: 23 March 2022

Nishimura, K. and Nemoto, M.: Blowing snow at Mizuho station, Antarctica, Philosophical Transactions of the Royal Society A: Mathematical, Physical and Engineering Sciences, 363, 1647–1662, https://doi.org/10.1098/rsta.2005.1599, 2005.

Nishimura, K., Yokoyama, C., Ito, Y., Nemoto, M., Naaim-Bouvet, F., Bellot, H., and Fujita, K.: Snow particle speeds in drifting snow, Journal of Geophysical Research: Atmospheres, 119, 9901–9913, 2014.

Paulcke, W. and Welzenbach, W.: Schnee, Wächten, Lawinen, Zeitschrift für Gletscherkunde, Eiszeitforschung und Geschichte, 16, 49–69, 1928.

Pomeroy, J. and Gray, D.: Saltation of snow, Water resources research, 26, 1583–1594, https://doi.org/10.1029/WR026i007p01583, 1990.

Schleef, S., Jaggi, M., Löwe, H., and Schneebeli, M.: An improved machine to produce nature-identical snow in the laboratory, Journal of Glaciology, 60, 94–102, https://doi.org/10.3189/2014JoG13J118, 2014.

Seligman, G., Seligman, G. A., and Douglas, C.: Snow structure and ski fields: being an account of snow and ice forms met with in nature, and a study on avalanches and snowcraft, Macmillan and Company, limited, 1936.

Sommer, C. G., Lehning, M., and Fierz, C.: Wind tunnel experiments: saltation is necessary for wind-packing, Journal of Glaciology, 63, 950–958, https://doi.org/10.1017/jog.2017.53, 2017.

Sommer, C. G., Lehning, M., and Fierz, C.: Wind tunnel experiments: influence of erosion and deposition on wind-packing of new snow, Frontiers in Earth Science, 6, 4, https://doi.org/10.3389/feart.2018.00004, 2018.

Sørensen, M.: On the rate of aeolian sand transport, Geomorphology, 59, 53–62, https://doi.org/10.1016/j.geomorph.2003.09.005, 2004.

Sugiura, K., Nishimura, K., Maeno, N., and Kimura, T.: Measurements of snow mass flux and transport rate at different particle diameters in drifting snow, Cold Regions Science and Technology, 27, 83–89, https://doi.org/10.1016/S0165-232X(98)00002-0, 1998.

Takeuchi, M.: Vertical profile and horizontal increase of drift-snow transport, Journal of Glaciology, 26, 481–492, https://doi.org/10.3189/S0022143000010996, 1980.

Tsutsumi, T.: Relationship between Snow Cornice on Flat Roof and Meteorological Element, Journal of Snow Engineering of Japan, 21, 317–320, https://doi.org/10.4106/jsse.21.5_317, 2005.

van Herwijnen, A. and Fierz, C.: Monitoring snow cornice development using time-lapse photography, in: Proceedings of the International Snow Science Workshop, pp. 865–869, 2014.

Veilleux, S., Decaulne, A., and Bhiry, N.: Snow-cornice and snow-avalanche monitoring using automatic time-lapse cameras in Tasiapik Valley, Nunavik (Québec) during the winter of 2017-18, Arctic Science, https://doi.org/10.1139/as-2020-0013, 2021.

Vogel, S., Eckerstorfer, M., and Christiansen, H. H.: Cornice dynamics and meteorological control at Gruvefjellet, Central Svalbard, The Cryosphere, 6, 157–171, https://doi.org/10.5194/tc-6-157-2012, 2012.

Wahl, L., Planchon, O., and David, P.-M.: Characteristics and seasonal evolution of firns and snow cornices in the High Vosges mountains (eastern France), Erdkunde, pp. 51–67, https://doi.org/10.3112/erdkunde.2009.01.04, 2009.

Walter, B., Horender, S., Voegeli, C., and Lehning, M.: Experimental assessment of Owen's second hypothesis on surface shear stress induced by a fluid during sediment saltation, Geophysical Research Letters, 41, 6298–6305, 2014.

Zhizhong, Z. and Wenti, W.: Primary Observations of the Deformation of Snow Cornice, Journal of Glaciology and Geocryology, p. 03, 1987.